Chronology of Accessory Phases in Lunar Meteorite Northwest Africa 12593. C. A. Crow[1], R. Economos[2], K. Lehman[2], S. Pomeroy[1], T. Erickson[3], M. Brounce[4] and J. Boyce[3], [1]University of Colorado Boulder (carolyn.crow@colorado.edu) , [2]Southern Methodist University, [3]NASA Johnson Space Center, [4]University of California Riverside.

Introduction: Lunar meteorites are complementary to the suite of rock and regolith samples collected by the Apollo missions. While the Apollo samples represent the most pristine material we have from the Moon, lunar meteorites represent a more global sampling of the lunar crust, albeit without geologic context [e.g. 1]. As such, lunar meteorites are important for understanding the composition of the lunar crust and the processes responsible for its formation and evolution.

This work aims to understand the observed differences in accessory phase chronology and volatile chemistry between lunar meteorites and Apollo rocks. For example, apatite ages in Apollo samples range from ~3.83 to 4.28 Ga [e.g. 2, 3], while apatites in lunar meteorites range from ~3.00 to 4.44 Ga [e.g. 4, 5]. Additionally, a much larger range of Cl isotope compositions and concentrations is observed in lunar meteorites as compared to Apollo samples [e.g. 6]. It has recently been shown that impact metamorphism can influence both chronology and chemistry of phosphates [e.g. 7, 8].

Here we present the first chronologic results from a consortium study pairing chronology, volatile chemistry, and crystal structure of apatites in a lunar breccia meteorite. The results of this work will help inform interpretation of ongoing analyses of apatites separated from Apollo soils.

Sample: NWA 12593 is a clast-rich, lunar fragmental breccia meteorite found in Mali. The meteorite has abundant clasts including basaltic, granulite, and crystalline impact melt, embedded in a fine-grained matrix [9]. It is moderately altered and may be moderately shocked [9, 10]. Previous studies have analyzed the Cl and H isotope composition of apatites from NWA 12593 [11]. The H and Cl isotopes are mainly within the range of Apollo samples (+10‰ to +24‰), however there is a subset of grains with high δ^{37}Cl (~ +55‰).

We obtained a 4.48 g slice of NWA 12593 that contains abundant mineral fragments and small lithic clasts and only a few larger clasts. Our section is therefore dominated by fine-grained impact melt matrix (Fig. 1).

We identified 66 apatites, 105 merrillites, 21 baddeleyites, and two zircons. There are some large grains up to ~100 μm, however, most are small with grainsizes <30μm. This abstract focuses on the apatite and baddeleyite grains. The apatites are mainly found in the fine-grained matrix, however some are in clasts; the baddeleyites are found both in the matrix as well as associated with apatite and merrillites in small clasts (Fig. 2). Only clast baddeleyites were analyzed herein.

Methods: Here we summarize the analyses that have been conducted thus far as part of a consortium effort. The original specimen was divided into three sub-sections, each of which were mounted in 1-inch epoxy rounds (Fig. 1), and polished for EBSD analyses. Microstructural EBSD analyses of apatite and baddeleyite grains was collected at NASA JSC using a 7900F Scanning Electron Microscope (SEM). Sulfur oxidation state of apatites has been assessed via XANES using the Advanced Photon Source at Argonne National Laboratory, the results of which are summarized in (Brounce et al., LPSC 2022). For some samples, EBSD was performed prior to XANES to test for electron beam effects on sulfur oxidation state. Relative sulfur concentrations of apatites were assessed wavelength dispersive spectroscopy (WDS) using the ThermoFisher Magnarary Spectrometer mounted on the JEOL-IT500HR Field Emission SEM at Southern Methodist University. Elemental maps of the sections were collected using the JEOL JXA-8230 electron microprobe at the University of Colorado Boulder (Fig. 2). Finally, ^{207}Pb-^{206}Pb geochronology was measured for a subset of apatite and baddeleyite grains using the Cameca ims1290 at the University of California, Los Angeles. Samples were analyzed with the Hyperion II ion source using a 5nA $^{16}O^-$ primary beam and ~10μm spot size.

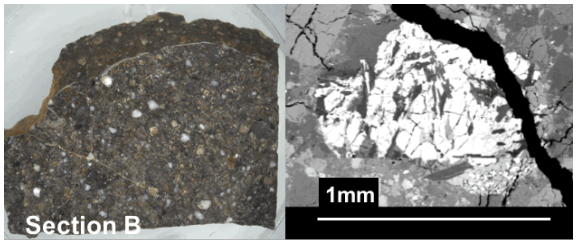

Fig 1: (Left) section of NWA 12593 in 1-inch epoxy rounds. (Right) symplectite clast in NWA 12593.

Results: The focus of this abstract is the chronology and electron beam analyses of NWA 12593 apatites and baddeleyites. Sulfur oxidation analyses can be found in [10], however, we note that these analyses appear to be significantly influenced by terrestrial alteration.

Electron Beam Methods. EBSD analyses were collected for all apatite, merrillite, baddeleyite, and zircon grains. This full dataset is currently being processed. All apatite grains were surveyed via WDS wavelength scan and four exhibited S peaks significant above background. All four of these grains are located in the fine-grained matrix.

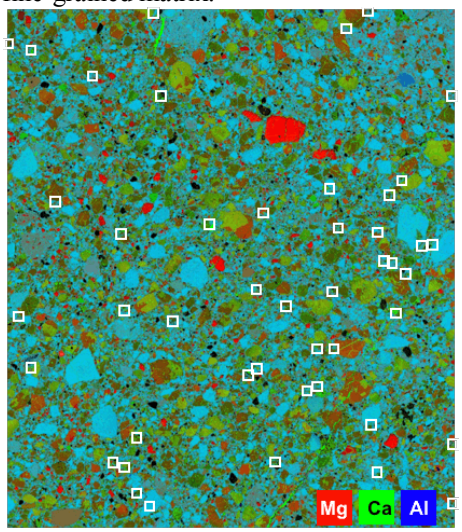

Fig 2: Elemental map of NWA 12593 Section C showing location of apatite, merrillite, and baddeleyite grains. Most are located within the fine-grained matrix

SIMS Pb-Pb Chronology. Pb isotopes were collected for 12 apatites and two baddeleyite grains, with four grains being large enough to have two SIMS spots each. The results are shown in the inverse isochron diagram in Fig. 3. Four analyses were excluded because of high abundances of mineral inclusions within the analysis locations.

There are multiple analyses with negligible ^{204}Pb (including one baddeleyite grain), thus these grains are interpreted to give robust crystallization ages. Three of these low-^{204}Pb grains are located within the fine-grained matrix; two of which cluster with similar ^{207}Pb/^{206}Pb ratios and give a weighted average ^{207}Pb-^{206}Pb age of 3493 ± 20 Ma (2σ). However, there is one apatite (Section C-Ap10) that has negligible ^{204}Pb and gives a ^{207}Pb-^{206}Pb age of 4334 ± 28 Ma (2σ). There are also two other grains with low-^{204}Pb, an apatite and baddeleyite from a symplectite clast. These grains give a weighted mean age of 3486±17 (2σ), which is indistinguishable within uncertainty from the matrix apatites.

All other analyzed grains are consistent with an ~3.49 Ga crystallization age with varying contributions from non-radiogenic lunar and terrestrial Pb. There are two grains (red ellipses) in Fig. 3 that either require a KREEP-type, high-μ Pb component or an older crystallization age [12]. The high-S apatites (blue ellipses) appear to fall on a mixing line that potentially suggests a separate initial-Pb reservoir, however these could also be explained by mixing between a higher-μ reservoir and non-lunar Pb. Additional analyses of Pb-isotopes of other phases within clasts and matrix are necessary to determine the number of reservoirs represented in this sample.

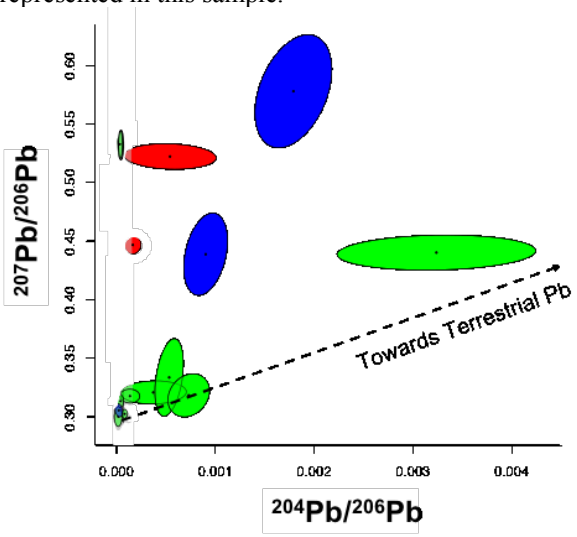

Fig 3: Inverse isochron diagram for NWA 12593 apatite and baddeleyite grains. Red ellipses require high-u (KREEP) initial Pb. Blue ellipses are high-S apatites.

Discussion: The old ages for low-^{204}Pb apatite C-Ap10 paired with the symplectite clast age suggests NWA 12593 contains materials ranging from 3486±17 (2σ) to 4334 ± 28 Ma (2σ). This further supports previous observations of the diversity of crustal materials found in this sample [9].

The apatites in this study are primarily found in the fine-grained matrix and have an age indistinguishable from that of the symplectite clast. This suggest that either (1) the matrix grains reflect the breccia formation event and the clast formed just prior to this event; (2) the matrix grains are sourced from target rocks of similar age to clast material and are not disturbed by the brecciation event; or (3) the breccia formation disturbed the Pb-systematics of both clast and breccia grains. Integration of the EBSD analyses will shed light on the extent of possible impact resetting or disturbance.

References: [1] Gross J. et al. (2014) *EPSL, 388,* 318-328. [2] Nemchin A. A. (2016) [3] Nemchin A. A. (2020). [4] Terada et al. (2017) [5] Wu and Hsu (2020). [6] Lin Y. and van Westrenen W. (2019) *NSR,* 6, 1247-1254. [7] Joy K. H. et al. (2011) *GCA,* 75, 2420-2452. [8] Černok A. et al. (2019). *LPSC L*, Abstract #2232. [9] Meteoritical Bulletin, no.108 (2020) *MAPS*, 55, 1146-1150. [10] Brounce M. (2022) *LPSC LIII*. [11] Hayden T. S. et al. (2021) *LPSC LII*, Abstract #1550. [12] Snape J. F. (2016) *EPSL*, 451, 149-158.